Supplemental Information for "Spherical aberration correction in nonlinear microscopy and optical ablation using a transparent deformable membrane".

Lens Fabrication. The membrane is fabricated from a customized formulation of polydimethilsyloxane (PDMS); parts A and B of RTV615 (General Electric) are mixed in a proportion of 25:1 as compared to the 10:1 ratio that is recommended by the manufacturer. The increased ratio produces an elastomer with a substantially reduced Young's modulus, *i.e.*, ~ 0.2 MPa compared to ~ 2 Mpa, and at least a 70 % increase in extensibility.

To form a 1.5 thick membrane, 10 g of the PDMS pre-polymer is poured onto a pre-leveled, 4 inch diameter silicon wafer. As a means to insure a uniformly flat membrane, the wafer is placed on a horizontal tilt stage, and its center is illuminated by a parallel beam of Helium-Neon laser light, ~10 mm in diameter, that is directed nearly perpendicular to the wafer surface. The interference pattern produced by the reflections from the surfaces of the wafer and the PDMS layer is projected onto a screen. The number of interference fringes is iteratively minimized by adjustment of the tilting stage to cause the pre-polymer to slowly flow and change its thickness profile as it gradually cures at room temperature. After a few hours of level adjustment, the PDMS is left to cure overnight. The final membrane typically produces one interference fringe, corresponding to a wedge-shaped thickness variation of ~ 0.25 μm per 10 mm.

To complete the curing of PDMS, the wafer is baked for 5 hours at 50 ° C and then the membrane is affixed to an acrylic mount. The mount has a shape of a ring with a 25 mm outer diameter, a 12 mm inner diameter, and a 1 mm wide circular groove on the front face that enhances the bonding of the membrane to the mount. The groove is connected to the back face of the mount by two through-holes, and there is a tapped hole in a side wall of the mount for an insert that connects the interior of the mount to a vacuum line. The front face of the mount is dipped onto a 100 μm thick layer of the same PDMS pre-polymer spin-coated on the surface of a different silicon wafer. The

mount is then placed onto the center of the cured membrane, and the wafer with the membrane and the mount are baked for 2 hours at 50° C to fix the mount on the membrane. The PDMS pre-polymer is slowly injected into the groove with a syringe needle through one of the two through-holes, and the entire assembly is further baked overnight at 50° C oven to completely cure the PDMS. The membrane is excised with a knife along the outer diameter of the mount, separated from the wafer, and a 22 mm round no. 2 microscope cover glass is attached with cyanoacrylate (Superglue) to the back face of the mount. The entire assembly is mounted into a linear translation stage (Fig. 1a).

Imaging. Images of fluorescent beads are acquired in an over-sampling configuration of 4 voxels per micrometer axially and 20 voxels per micrometer laterally across a 12 μm field. The distribution of fluorescence in a three-dimensional sub-region around each bead is extracted, and each frame in the z-axis stack is filtered with a two-dimensional 7x7 pixel Gaussian filter (5 pixel full-width-at-half-maximum). The maximum value of intensity for each frame is plotted against the z-axis position, and the full-width-at-half-maximum of the curve is reported as the axial resolution.

Ablation Visualization. Femtosecond pulse laser ablation damage is visualized using wide-field transmitted and epi-illumination. The glass slides used as the ablation targets are separated and turned by their unpolished edge to face a 20X, 0.75 NA air objective (Fig. 4b). In this configuration, the axial dimension of the ablated regions lies in the imaging plane of the air objective and thus the axial extension of the ablation can be imaged at a high resolution. The slides are sandwiched between similarly oriented blank slides, index-matching immersion oil is applied to the unpolished edges to mask their roughness, and an ∼ 0.1-mm thick no. 0 cover slip is placed atop the surface to provide aberration-free imaging of the damage region. Scattered light images are captured on a CCD camera (Apogee KX32ME) and analyzed by visual inspection.

Model of the Microscope Objective. The detailed schematics for commercial water-dipping objectives are not available. Therefore, to analyze the effect of placing a curved transparent membrane behind a microscope objective, we model the objective by a plano-convex aspheric lens oriented with its planar face towards the focus (Fig. S1). The shape of the aspheric lens is derived from the condition that the focus of a plane wave parallel to the optical axis is free of spherical aberration. This condition constrains the choice of parameters of the lens, *i.e.*, the center thickness, T_o, and the distance from the planar face to the frontal focal plane, f, the refractive index of the input medium at the curved surface, n_1, the index of the lens material, n_2, and the index of the output medium at the planar surface, n_3.

The shape of the lens can be specified by its thickness as a function of radius, T(R). To find the lens shape, it is convenient to follow a ray that is incident on the curved lens surface, traverses the lens, and exits the planar lens surface of the lens with a focusing angle, θ. For algebraic simplicity, we re-parameterize the lens shape in terms of the focusing angle, and derive the associated lens thickness, $T(\theta)$, and the incident radius, $R(\theta)$ (Fig. S1).

The angle of a ray inside the lens, θ', is defined relative to the optical axis and is related to the focusing angle, θ by Snell's, law, *i.e.*,

(1) $\qquad n_2 \sin(\theta') = n_3 \sin(\theta)$.

We consider only input rays that are parallel to the optical axis. We apply Fermat's principle and require that the optical path between the back plane of the lens, at $z = z_i$, and the focal point, at $z = z_f$, at be the same for all rays. For purposes of calculation, we equate the optical path of a given ray with the optical path of the ray directed on the optical axis,

. (2) $\qquad n_1 d_1 + n_2 d_2 + n_3 d_3 = n_2 T_0 + n_3 f$.

where the parameters d_1, d_2, and d_3 are the physical path lengths along the ray through the input medium, the lens, and the output medium, respectively. These three distances are expressed in terms of T_o, f, θ, θ' and $T(\theta)$, *i.e.*,

(3) $\quad d_1 = T_0 - T(\theta)$

(4) $\quad d_2 = T(\theta)/\cos(\theta')$

(5) $\quad d_3 = f/\cos(\theta)$

We use the trigonometric equality $\cos(\theta') = \sqrt{1 - \sin^2(\theta')}$ and equation 1 to obtain

(6) $\quad \cos(\theta') = \sqrt{1 - \left(n_3/n_2\right)^2 \sin^2(\theta)}$.

Substitution of equations 3 to 6 into equation 2 yields

(7) $\quad n_1\left[T_0 - T(\theta)\right] + n_2 T(\theta)\Big/\sqrt{1 - \left(n_3/n_2\right)^2 \sin^2(\theta)} + n_3 f/\cos(\theta) = n_2 T_0 + n_3 f$.

We solve equation 7 for the lens thickness, $T(\theta)$, yields

(8) $\quad T(\theta) = \dfrac{(n_2 - n_1)T_0 - n_3 f\left\{\left[1/\cos(\theta)\right] - 1\right\}}{\left[n_2\Big/\sqrt{1 - \left(n_3/n_2\right)^2 \sin^2(\theta)}\right] - n_1}$.

We next obtain R(θ) from simple geometrical considerations. We consider the ray associated with the angle θ. The radial distance at which this ray intercepts the planar lens surface, denoted by $R_2(\theta)$, is given by (Fig. S1):

(9) $\quad R_2(\theta) = f \tan(\theta)$

and the difference between R(θ) and $R_2(\theta)$, denoted by ΔR(θ), is given by:

(10) $\quad \begin{aligned} \Delta R(\theta) &= T(\theta)\tan(\theta') \\ &= T(\theta)\sin(\theta')\Big/\sqrt{1 - \sin^2(\theta')} \\ &= T(\theta)\left(n_3/n_2\right)\sin(\theta)\Big/\sqrt{1 - \left(n_3/n_2\right)^2 \sin^2(\theta)} \end{aligned}$.

Finally, using R(θ) = $R_2(\theta)$ + ΔR(θ) and equation 8 to specify T(θ), we obtain:

(11) $\quad R(\theta) = f\tan(\theta) + \left(\dfrac{n_3}{n_2}\right)\dfrac{\left[(n_2 - n_1)T_0 + n_3 f\right]\sin(\theta) - n_3 f\tan(\theta)}{n_2 - n_1\sqrt{1 - \left(n_3/n_2\right)^2 \sin^2(\theta)}}$.

Equation 11 and the values of the parameters T_0, f, n_1, n_2, and n_3 uniquely define the shape of the aspheric lens, with the constraint that the set of parameters must satisfy R(θ) > 0 ∀ θ.

Model of the Membrane. We model the shape of the deformable membrane with the equation for a thin deformable membrane with clamped edges[1]. The axial displacement of the membrane as a function of the radial position, z(r) is given by:

$$z = \frac{9}{64}\frac{r_o^4}{Eh^3}\Delta P \left[\left(1 - \frac{r^2}{r_o^2}\right)\right]^2$$

(12)

$$\equiv \eta \left[\left(1 - \frac{r^2}{r_o^2}\right)\right]^2$$

where E is the elastic modulus, h is the thickness, and r_o is the radius of the membrane. The pressure difference across the membrane is ΔP. As the fabricated membrane is only approximately thin, *i.e.*, h/r = 0.25, the first surface of the membrane is modeled by equation 12 and the second surface is constrained to lie a distance h along the perpendicular to the first surface. For purposes of curve fitting (Fig. 1C), all of the prefactors at constant ΔP are grouped into a singe term, denoted η (Eqn. 12).

Ray Tracing. First, we performed geometric ray tracing of the aspheric lens defined by equation 11 with the parameters set at values of T_o = 2.5 mm, f = 3.6 mm, n_1 = 1.00, n_2 = 1.76, and n_3 = 1.33. The maximum radius was R(θ_{max}) = 3.3 mm, which matches the back aperture and numerical aperture of the objective. As noted in our derivation (Eqs. 2 to 6), we take the input beam to be collimated light that is parallel to the optical axis. By construction, the lens produces a geometrically perfect focus in a homogenous output medium (Figs. S2a and S2b). We then introduced a flat interface with a medium of a higher refraction index, n_4 = 1.42, at 3.2mm in front of the lens, to emulate focusing at a mean depth of 0.45 mm into agarose gel and cleared biological tissue, as used in the study (Figs. 2 and 3). Refraction at the interface results in a positive spherical aberration, wherein marginal rays are focused further from the lens than paraxial rays (Figs. S2c and S2d). This is the aberration that we seek to compensate with our membrane.

We used ray tracing to evaluate the effect of non-collimated input to the aspheric lens. We first consider perfectly converging/diverging rays that originates at a geometric point; this corresponds to a divergent lens placed behind the objection that is free of aberration. We find that perfectly converging input to the aspheric lens produces a focus in the homogenous output medium with positive spherical aberration (Figs. S2e and S2f). Conversely, perfectly diverging input on the aspheric lens produces a focus in the homogenous output medium with negative spherical aberration, wherein marginal rays are focused closer to the lens than paraxial rays. Thus a diverging input to the aspheric lens leads a negative spherical aberration that counteracts the positive aberration induced by a higher index interface in the output medium.

We performed geometric ray tracing of the deformable membrane (Eq. 12) using parameter values of $\eta = 0.60$ mm and $r_o = 7.04$ mm. The central region of the membrane acts as a diverging lens with negative spherical aberration. Towards its outer rim, the membrane acts as a converging lens with negative spherical aberration (Fig. S3a). Ray tracing through an optical system that consists of a deformable membrane, an aspheric lens, and a higher-index interface (Fig. S3b and S3c) shows an improvement of the focus compared the focus generated through a higher-index interface without the deformable membrane (*cf* Figs. S2b and S3c).

As a means to quantify the quality of the focus, we represent the axial spread of the focus as the standard deviation of the intersection point of each ray with the optical axis, *i.e.*,

(13) $$\sigma = \sqrt{\frac{1}{N-1}\sum_{i=1}^{N}\left(f_i - \langle f \rangle\right)^2}$$

where f_i is the axial position at which the i-th geometric ray crosses the optical axis, $\langle f \rangle$ is average of all crossing positions, and N is the number of rays considered. By this metric, we find that the focus restoration by the modeled deformed membrane is improved compared to restoration with perfectly divergent lens (*cf* Figs. S2f and S3c). Thus both the divergence and negative spherical aberration of the membrane are compensating factors.

[1] L. D. Landau and E. M. Lifshitz, *Theory of Elasticity* (Pergamon Press, Oxford, 1959).

Figure Captions

Figure S1. Aspheric lens model for on-axis behavior of microscope objective. A cross-section of the aspheric lens is shown in blue. The indices of refraction of the input-side media, the lens material, and the output-side media are denoted as n_1, n_2, and n_3, respectively. The optical path of an off-axis ray is shown in red. The physical path lengths of an off-axis ray are denoted as d_1, d_2, and d_3. The radial position of the off-axis ray at the front and rear lens faces are denoted as $R(\theta)$ and $R_2(\theta)$, respectively, where θ is the focusing angle of the ray. The angle of the off-axis ray within the lens with respect to the optical axis is denoted as θ'. The center thickness of the lens is denoted as T_o, and the thickness of the lens at the entry position of the off-axis ray is denoted as $T(\theta)$. The distance from the lens rear surface to the focal plane is denoted as f.

Figure S2. Ray tracing of model objective. **(a)** Ray tracing of the model aspheric lens designed for use with air on the incident side and water only on the sample side (Fig. S1 and Eqn. 11). The field is 16 by 16 mm. **(b)** Enlarged view of the focusing region in panel (a). The field is 60 by 60 μm. **(c)** The same lens as in part (a), but with an intermediate interface into a higher-index material. **(d)** Enlarged view of the focusing region in panel (b). **(e)** The same lens and interface as in (b), but with the incident beam slightly divergent, formed by placing a point source 520 mm behind the objective. **(d)** Enlarged view of the focusing region in panel (e).

Figure S3. Ray tracing of model objective with membrane compensator. **(a)** Ray trace of the inflated membrane at an exaggerated inflation to illustrate the increased divergence of paraxial ray as compared to marginal rays. **(b)** Ray tracing of a model aspheric lens (Fig. S1 and Eqn. 11) with the membrane placed a distance 5 mm behind the objective. The field is 16 by 16 mm. **(c)** Enlarged view of the focusing region in panel (b). The field is 60 by 60 μm.
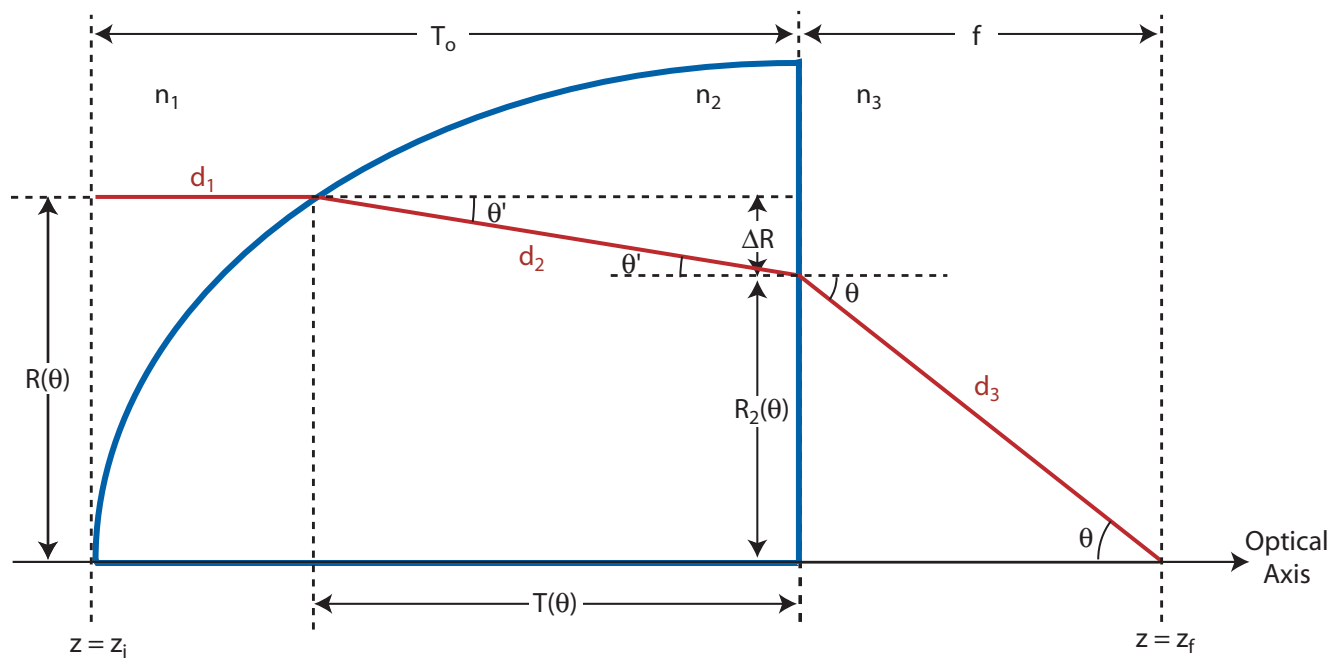
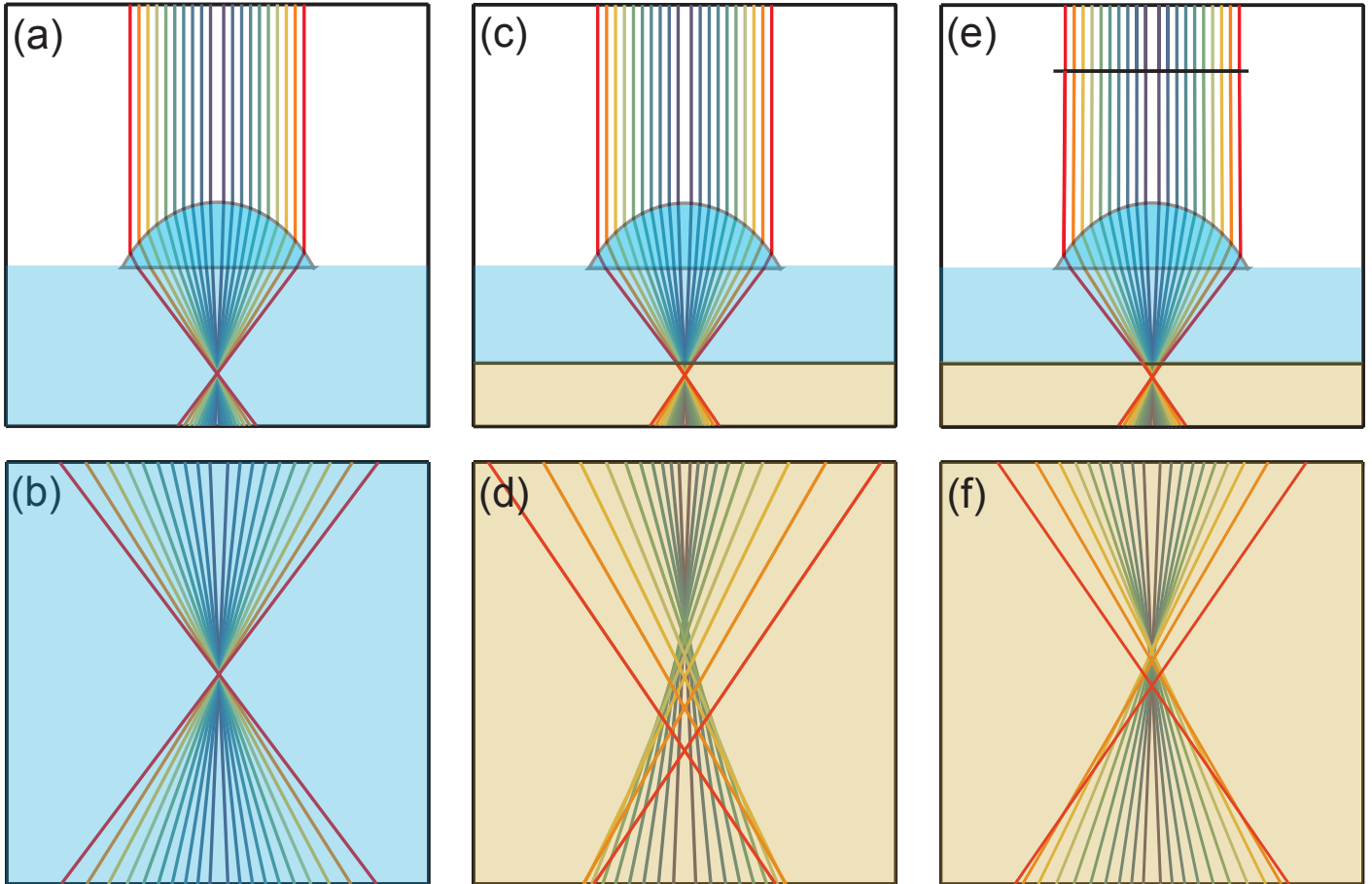Figure S1. Tsai, Migliori, Campbell, Kim, Kam, Groisman and Kleinfeld

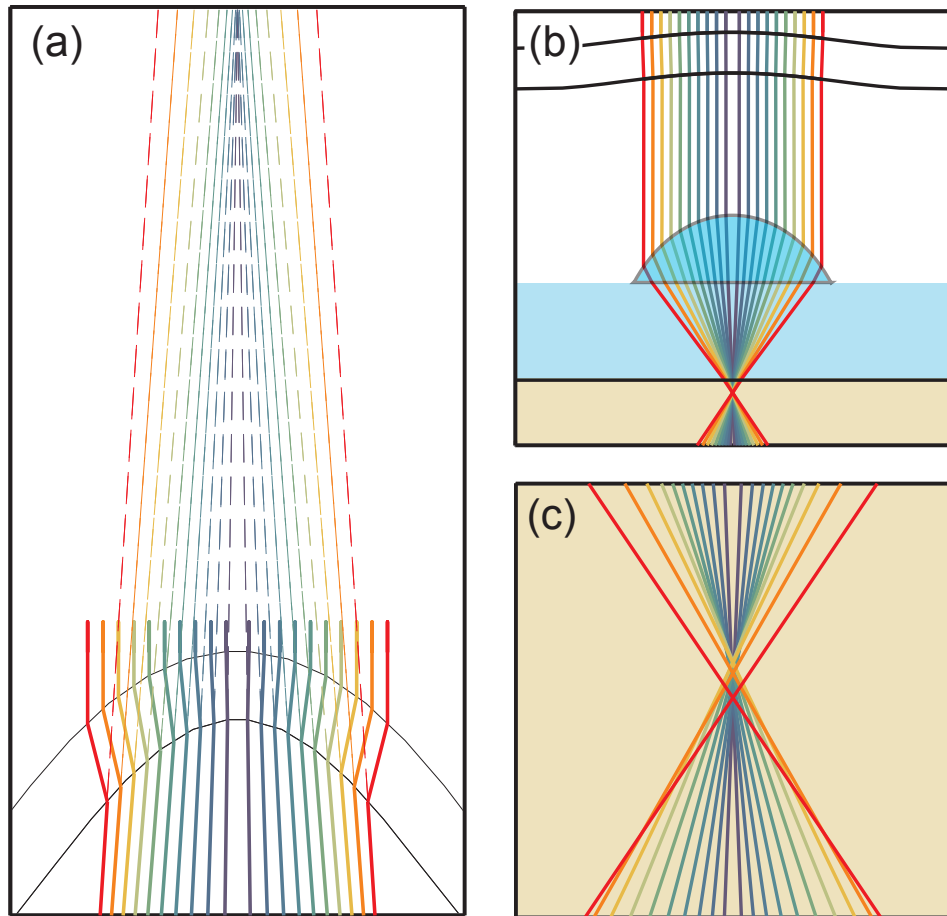Figure S2. Tsai, Migliori, Campbell, Kim, Kam, Groisman and Kleinfeld

Figure S3. Tsai, Migliori, Campbell, Kim, Kam, Groisman and Kleinfeld